Linear instability of pressure-driven channel flow of a Newtonian and a Herschel-Bulkley fluid

K. C. Sahu, P. Valluri, P. D. M. Spelt and O. K. Matar

Department of Chemical Engineering,

Imperial College London, SW7 2AZ, UK

(Dated: September 28, 2007)

Abstract

The linear stability characteristics of pressure-driven two-layer channel flow are considered, wherein a Newtonian fluid layer overlies a layer of a Herschel-Bulkley fluid. A pair of coupled Orr-Sommerfeld eigenvalue equations are derived and solved using an efficient spectral collocation method for cases in which unyielded regions are absent. An asymptotic analysis is also carried out in the long-wave limit, the results of which are in excellent agreement with the numerical predictions. Our analytical and numerical results indicate that increasing the dimensionless yield stress, prior to the formation of unyielded plugs below the interface, is destabilising. Increasing the shear-thinning tendency of the lower fluid is stablising.

I. INTRODUCTION

In several applications, layers of highly-viscous fluids are displaced by another fluid. In the cleaning of fast-moving consumer good plants, for example, a highly viscous fluid is removed by pumping water through the plant. A common feature of the rheology of these fluids is the appearance of a yield stress. This concept has been challenged in several studies, but remains a very useful approximation (see [1] for an extensive review, and [2] for recent detailed measurements). In this paper, we study the stability of a fluid that exhibits a finite yield stress superposed by a Newtonian fluid, as shown in Fig. 1. A yield stress may affect the growth of interfacial waves, which ultimately would influence the rate at which the highly-viscous layer is removed.

Some relevant key features of the linear stability of planar two-fluid Poiseuille flow are briefly reviewed here; an extensive review can be found in [3]. The early work of Yih [4], who considered the stability of this flow to two-dimensional long-wave disturbances, elucidated the origin of the interfacial instability. Yih used an asymptotic analysis to derive an expression for the complex wave speed as a function of the relevant system parameters such as the density, viscosity and thickness ratios. He then demonstrated that instability exists due to an interfacial mode which results from a viscosity stratification even in the limit of vanishingly small Reynolds numbers. Yiantsios and Higgins [5] subsequently showed numerically the appearance of a shear mode at sufficiently large Reynolds numbers, which corresponds to a short-wave Tollmien-Schlichting mode.

Yiantsios and Higgins [6] also carried out an asymptotic analysis and extended the work of Yih to cover large wave numbers and to account for the effects of gravity and interfacial tension using the perturbation scheme of Hooper and Boyd [7]; the latter authors examined the short-wave asymptotics of the interfacial instability between two unbounded viscous fluids. They provided predictions of critical Reynolds numbers for both the shear and interfacial modes and demonstrated the existence of discrepancies between these predictions and the experimental data of Kao and Park [8]. They also compared their results with the weakly nonlinear evolution of the interface considered by Hooper and Grimshaw [9].

The stability of inelastic non-Newtonian fluids has been studied before (the extensive literature on the stability of elastic fluids **- see, for instance, Refs. [10–15]** - is not reviewed here). Most relevant here is a previous study by Frigaard [16] on the linear stability

of two-layer Poiseuille flow of two Bingham fluids. In the flows considered there, the shear stress distribution is assumed to be such that only a fraction of the Bingham fluid has yielded. In the present configuration, this would amount to an unyielded region between the Newtonian fluid and the yielded part of the Bingham fluid, hence interfacial waves would not develop under such conditions. This suppression of interfacial modes then leads to super-stable two-layer flows [16]. The flow would be increasingly stable at larger values of the yield stress, similar to single-fluid pressure-driven flows [17] (this was also noticed by Pinarbasi and Liakopoulos [18], but they used a regularised rheological model).

This previous work, however, does not address the stability of flows of a Newtonian fluid parallel to a Bingham fluid at flow rates sufficient for the entire Bingham fluid to yield (in a linear analysis), which would be appropriate for applications wherein the applied pressure gradient is simply too large. Also of practical relevance are situations in which fluids exhibit shear-thinning or shear-thickening behaviour; this is commonly represented by so-called 'Herschel-Bulkley' (HB) models, which incorporate the presence of a yield stress as well as power-law behaviour. The linear stability of an interface separating a Newtonian and Herschel-Bulkley fluid in pressure-driven channel flow has only been partially studied previously, primarily using long-wave approximations, for power-law fluids. Khomami [19, 20] showed through an asymptotic analysis in this limit that a regularised power-law model with a low-shear-Newtonian plateau should be used, otherwise the predictions would be misleading at low thickness ratios. Pinarbasi and Liakopoulos [18] also solved the Orr-Sommerfeld problem for HB fluids, but only for cases where the shear rate is insufficient for the HB fluid to yield everywhere, as mentioned above; they also only explore very low Reynolds numbers.

In order to address the important issues not addressed in previous work, as highlighted by the review presented above, we solve here an Orr-Sommerfeld-type problem for the configuration shown in Fig. 1, for cases wherein the rheology of the non-Newtonian fluid can be represented by an HB model, and in the absence of unyielded regions under linear conditions (the subsequent nonlinear evolution may very well result in unyielded regions, but this is beyond the scope of this paper). Growth rates will be presented as a function of model parameters. Of particular interest is a conjecture proposed by Frigaard [16], that the variation in the local value of the viscosity is negligible on the scale of infinitesimal waves, such that the results are expected to be very similar to the corresponding problem

of two superposed Newtonian fluids. A reason to believe that this argument is of limited validity follows from the interpretation of the physical mechanism of interfacial instabilities proposed by Boomkamp and Miesen [3]. Those authors use an energy balance to show that such instability, when driven by a viscosity contrast, arises because of the discontinuity in shear rate across the interface. Evidently, this discontinuity is different for different values of the yield stress in a HB fluid. It is therefore of interest to study this problem in detail, which appears not to have been done previously.

The results of the numerical solution and a long-wave asymptotic analysis of this Orr-Sommerfeld eigenvalue problem show that increasing the yield stress (prior to the formation of unyielded regions) and the shear-thickening tendency of the non-Newtonian fluid promote instability. The results presented here also provide an important benchmark for full numerical simulations of these flows, using e.g. level-set or phase-field methods, for the study of the subsequent nonlinear evolution.

II. FORMULATION

A. Governing equations

We consider the two-dimensional flow of two-fluids in a channel driven by a constant pressure gradient in the streamwise direction. The upper and lower fluids are assumed to be Newtonian and non-Newtonian, respectively; both fluids are incompressible. We use a rectangular coordinate system to analyse the linear stability characteristics of this flow: x and y denote the streamwise and wall normal directions, respectively, as indicated in Fig. 1. The direction of the gravitational acceleration is assumed to be aligned with the $y-$axis. The lower and upper channel walls are located at $y = 0$ and $y = H$, respectively, and the sharp interface, which separates the immiscible fluids, is at $y = h$.

We have adopted the Herschel-Bulkley model to describe the rheological characteristics of the non-Newtonian fluid,

$$\mu_1 = k\Pi^{n-1} + \tau_0\Pi^{-1}, \tag{1}$$

where μ_1 is the apparent viscosity, k and n denote the consistency and flow index, and τ_0 the yield shear stress; $\Pi \equiv (2E_{ij}E_{ij})^{1/2}$ represents the second invariant of the rate of strain tensor, $E_{ij} = \frac{1}{2}(\partial u_i/\partial x_j + \partial u_j/\partial x_i)$. As explained in the Introduction, we restrict the

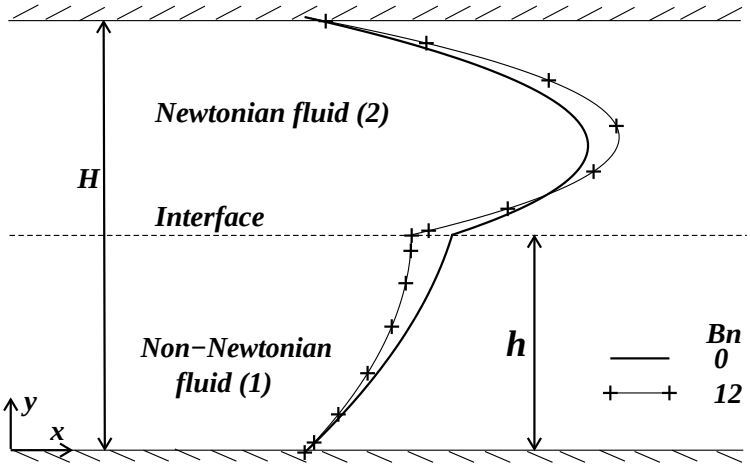

FIG. 1: Schematic of a two-layer flow in a channel of height H, where h represents the thickness of the lower, non-Newtonian fluid. Also shown here are profiles of the steady, streamwise velocity component generated with $Bn = 0$ and $Bn = 12$.

analysis to sufficiently low values of τ_0 so that there are no unyielded regions in $0 \leq y \leq h$.

Solutions of the equations of motion are sought subject to the no-slip and no-penetration conditions at the walls, continuity of the normal and tangential components of the velocity and stress fields, and the kinematic condition at the interface. These equations and boundary conditions are rendered dimensionless using the velocity scale, V, the channel height, H, and the density and viscosity of the upper fluid, ρ_2 and μ_2, respectively; they are not presented here for brevity. (The subscripts '1' and '2' are used to represent quantities associated with the lower and upper fluids, respectively.) The reduced dimensionless pressure P_i in fluid 'i' is related to the corresponding total dimensional pressure p_i through

$$P_i = \frac{H}{\mu_2 V}\left[p_i + \rho_i g(y-h)\right], \quad (i = 1, 2) \tag{2}$$

where g is the gravitational acceleration. This effectively transfers the hydrostatic term from the momentum conservation equations to the interfacial normal stress boundary conditions, as will be shown below. The dimensionless viscosity of the non-Newtonian fluid is

$$\mu_1 = m\Pi^{n-1} + Bn\Pi^{-1}, \tag{3}$$

where $Bn \equiv \tau_0 H/\mu_2 V$ is a Bingham number and $m \equiv \mu_2^{-1} k (V/H)^{n-1}$ is a viscosity ratio.

The base state corresponds to a steady and unidirectional velocity field in both layers,

driven by a linear pressure distribution in x ($P_1 = P_2 \equiv P$), for a flat interface:

$$U_1 = \frac{n}{n+1}\frac{(\mathrm{d}P/\mathrm{d}x)^{-1}}{m^{1/n}}\left[\frac{\mathrm{d}P}{\mathrm{d}x}y + c_3 - Bn\right]^{n+1/n} + c_4, \tag{4}$$

$$U_2 = \frac{\mathrm{d}P}{\mathrm{d}x}\frac{y^2}{2} + c_1 y + c_2. \tag{5}$$

The pressure gradient, $\mathrm{d}P/\mathrm{d}x$ and the integration constants, c_1, c_2, c_3, and c_4 are obtained by solving the following simultaneous equations

$$\frac{n(\mathrm{d}P/\mathrm{d}x)^{-1}}{(n+1)m^{1/n}}\left\{\left[\frac{\mathrm{d}P}{\mathrm{d}x}h + c_3 - Bn\right]^{n+1/n} - [c_3 - Bn]^{n+1/n}\right\} - \frac{1}{2}\frac{\mathrm{d}P}{\mathrm{d}x}\left(h^2 - 1\right) - c_1\left(h - 1\right) = 0,$$

$$c_3 = c_1, \quad c_2 = -\frac{1}{2}\frac{\mathrm{d}P}{\mathrm{d}x} - c_1, \quad c_4 = -\frac{n(\mathrm{d}P/\mathrm{d}x)^{-1}}{(n+1)m^{1/n}}\left[c_1 - Bn\right]^{n+1/n}, \tag{6}$$

$$\text{and} \quad \int_0^h U_1 dy + \int_h^1 U_2 dy = 1. \tag{7}$$

Equations (6) arise from imposing the no-slip conditions at the upper and lower walls and demanding continuity of velocity and stress at the interface, while Eq. (7) represents a condition of constant volumetric flow rate, $Q \equiv VH$.

In Fig. 1, it is seen that increasing the value of Bn leads to an increase in maximal velocity contrast between the upper and lower fluids. Our base state results also demonstrate (not shown) that decreasing (increasing) n below (above) unity, which corresponds to a shear-thinning (shear-thickening) fluid has the opposite effect. These features indicate that increasing n and Bn is expected to exert a destabilising influence on the flow.

B. Linear stability analysis

We investigate the stability of the base state characterised by U_1 and U_2 to infinitesimal, two-dimensional (2D) disturbances using normal modes by expressing each flow variable as the sum of a base state and a 2D perturbation:

$$(u_i, v_i, P_i)(x, y, t) = (U_i(y), 0, P) + (\hat{u}_i, \hat{v}_i, \hat{p}_i)(x, y, t), \tag{8}$$

with ($i = 1, 2$). Similarly the viscosity, μ_1, and h can be expanded as follows

$$\begin{aligned} \mu_1(\pi) &= \mu_1^0 + \left.\frac{\partial \mu_1}{\partial \pi}\right|^0 (\pi - \Pi) \equiv \mu_1^0 + \beta\hat{\pi}, \\ h(x,t) &= h^0 + \hat{h}(x,t), \end{aligned} \tag{9}$$

where $\beta = (n-1)m\Pi^{n-2} - Bn\Pi^{-2}$ and the superscript '0' designates base state quantities. Substitution of Eqs. (8) and (9) into the governing equations, subtraction of the base state equations and subsequent linearisation yields the equations that determine the linear stability of the flow cast in terms of primary variables. These equations are then re-expressed in terms of the streamfunction, $(u_i, v_i) = (\partial\Psi_i/\partial y, -\partial\Psi_i/\partial x)$ $(i = 1, 2)$ and the decomposition $\Psi(x, y, t) = \psi(y)e^{\mathrm{i}(\alpha x - \omega t)}$ is imposed, whence,

$$\begin{aligned}(\hat{u}_i, \hat{v}_i, \hat{p}_i, \hat{\pi})(x, y, t) &= (\psi_i', -\mathrm{i}\alpha\psi_i, p_i, \pi_i)(y)\mathrm{e}^{\mathrm{i}(\alpha x - \omega t)}, \\ \hat{h}(x, t) &= \eta e^{i(\alpha x - \omega t)}, \quad i = 1, 2. \end{aligned} \tag{10}$$

Here, ψ_i and η denote the amplitudes of the streamfunction and interfacial perturbation, respectively, α is a streamwise (real) wavenumber, $\omega(= \alpha c)$ is a complex frequency, c is a complex phase speed of the disturbance; the prime represents differentiation with respect to y. Note that $\omega_i > 0$ indicates the presence of a linear instability.

Eliminating the pressure perturbations in the usual way, yields the following coupled Orr-Sommerfeld-type equations,

$$\mathrm{i}\alpha r\mathrm{Re}\left[\left(\psi_1'' - \alpha^2\psi_1\right)(U_1 - c) - \psi_1 U_1''\right] = \mu_1^0[\psi_1'''' -$$

$$2\alpha^2\psi_1'' + \alpha^4\psi_1] + \beta U_1'\pi'' + 2\beta U_1''\pi' + \beta U_1'''\pi + \alpha^2\beta U_1'\pi -$$

$$-2\alpha^2\mu_1^{0'}\psi_1' + \mu_1^{0''}\psi_1'' + 2\mu_1^{0'}\psi_1''' + \beta'' U_1'\pi + 2\beta' U_1'\pi' + 2\beta' U_1''\pi + \mu_1^{0''}\alpha^2\psi, \tag{11}$$

$$\mathrm{i}\alpha\mathrm{Re}\left[\left(\psi_2'' - \alpha^2\psi_2\right)(U_2 - c) - \psi_2 U_2''\right] = \psi_2'''' - 2\alpha^2\psi_2'' + \alpha^4\psi_2, \tag{12}$$

where $r \equiv \rho_1/\rho_2$ is the density ratio and $\mathrm{Re} \equiv \rho_2 V H/\mu_2$ is the Reynolds number. In the limit $(n, Bn) \to (1, 0)$, these equations reduce to those used to study the stability of a two-layer Newtonian system [6].

The eigenvalue c and the eigenfunctions ψ_1 and ψ_2 are obtained via solution of Eqs. (11) and (12) subject to the following boundary conditions: the no-slip and no-penetration conditions at the walls:

$$\psi_1 = \psi_1' = 0, \qquad \text{at} \quad y = 0, \tag{13}$$

$$\psi_2 = \psi_2' = 0, \qquad \text{at} \quad y = 1; \tag{14}$$

continuity of the velocity components and of the normal and tangential stress components, and the kinematic condition at the interface:

$$\psi_1 = \psi_2, \tag{15}$$

$$\psi_1' - \psi_2' + \eta\left(U_1' - U_2'\right) = 0, \tag{16}$$

$$\psi_2'' - \alpha^2\psi_2 - {\mu_1}^0\left(\psi_1'' - \alpha^2\psi_1\right) = 0, \tag{17}$$

$$\begin{aligned}
&\alpha \mathrm{Re} r\Big[\psi_1'\left(c - U_1\right) + \psi_1 U_1'\Big] - \alpha \mathrm{Re}\Big[\psi_2'\left(c - U_2\right) + \psi_2 U_2'\Big] + \\
&2\mathrm{i}\alpha^2\left[\mu_1^0\psi_1' - \frac{3}{2}\psi_2'\right] + 2\mathrm{i}\alpha^2\mu_1^0\psi_1' - \mathrm{i}\Big[\mu_1^0\left(\psi_1''' + \alpha^2\psi_1'\right) + \\
&\mu_1^{0\prime}\left(\psi_1'' + \alpha^2\psi_1\right) + \beta U_1'\pi' + \beta' U_1'\pi + \beta U_1''\pi - \psi_2'''\Big] - \\
&\left(\Gamma\alpha^2 + \mathrm{G}\right)\alpha\frac{\left(\psi_1' - \psi_2'\right)}{\left(U_2' - U_1'\right)} = 0,
\end{aligned} \tag{18}$$

where η is readily determined to be

$$\eta = \psi_1/\left(c - U_1\right)|_h = \psi_2/\left(c - U_2\right)|_h. \tag{19}$$

Here, $G \equiv \left(\rho_1 - \rho_2\right) gH^2/\mu_2 V$ and $\Gamma \equiv \sigma/\mu_2 V$ represent a Bond number and an inverse capillary, respectively, in which case σ denotes the interfacial tension.

C. Numerical procedure and validation

Solutions of Eqs. (11)-(12) subject to boundary conditions (13)-(18) are obtained using the spectral collocation method [21]. The eigenfunctions, ψ_1 and ψ_2 are expanded using Chebyshev polynomials in the intervals [0-h^0] and [h^0-1] respectively. The eigenvalue problem is then re-cast into the following matrix form

$$\begin{bmatrix} \mathcal{A}_{11} & \mathcal{A}_{12} \\ \mathcal{A}_{21} & \mathcal{A}_{22} \end{bmatrix} \begin{bmatrix} \psi_1 \\ \psi_2 \end{bmatrix} = c \begin{bmatrix} \mathcal{B}_{11} & \mathcal{B}_{12} \\ \mathcal{B}_{21} & \mathcal{B}_{22} \end{bmatrix} \begin{bmatrix} \psi_1 \\ \psi_2 \end{bmatrix}, \tag{20}$$

and solved using the public domain software, LAPACK. A similar technique has previously been used to study the stability of flow through a pipe [22]. This procedure allows the numerical calculation of dispersion relations $\omega_i = \omega_i(\alpha; Bn, n, \mathrm{Re}, m, r, \Gamma, \mathrm{G})$.

The dependence of our numerical solutions upon mesh refinement is investigated in Fig. 2, in which we plot ω_i against α for Re $= 100$, $h^0 = 0.5$, $m = 10$, $r = 1.1$, $G = 10$, $\Gamma = 1$, $Bn = 4$ and $n = 1$. It is seen that the curves for different values of the order of Chebyshev polynomials, N, are virtually indistinguishable for $N \geq 61$. The results discussed in the rest of this paper were generated using $N = 101$.

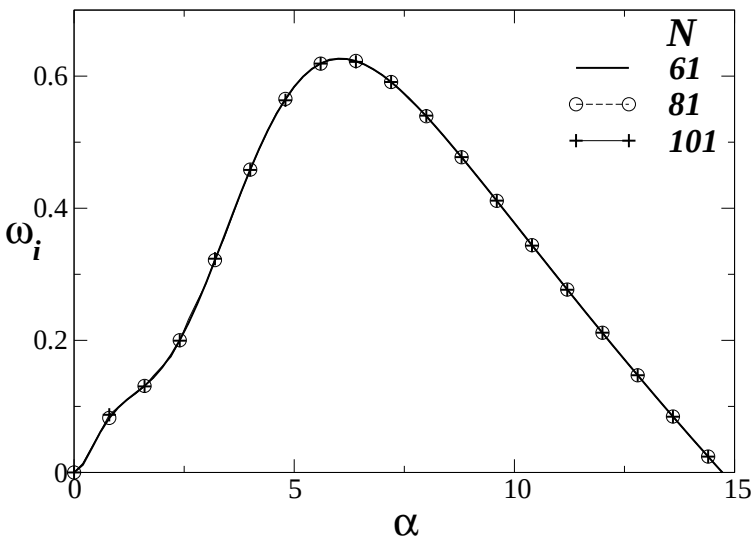

FIG. 2: The effect of increasing the order of Chebyshev polynomials, N, on the variation of ω_i with α with Re $= 100$, $h^0 = 0.5$, $m = 10$, $r = 1.1$, $G = 10$, $\Gamma = 1$, $Bn = 4$ and $n = 1$.

In order to validate the predictions of our numerical procedure, we have also made detailed comparisons with several published results for single and two-layer Newtonian flows. In Fig. 3, we compare our results with those of South and Hooper [23] (see Fig 4(c) in [23]) and find excellent agreement. Excellent agreement is also found with the work of Yiantsios and Higgins [6] (not shown).

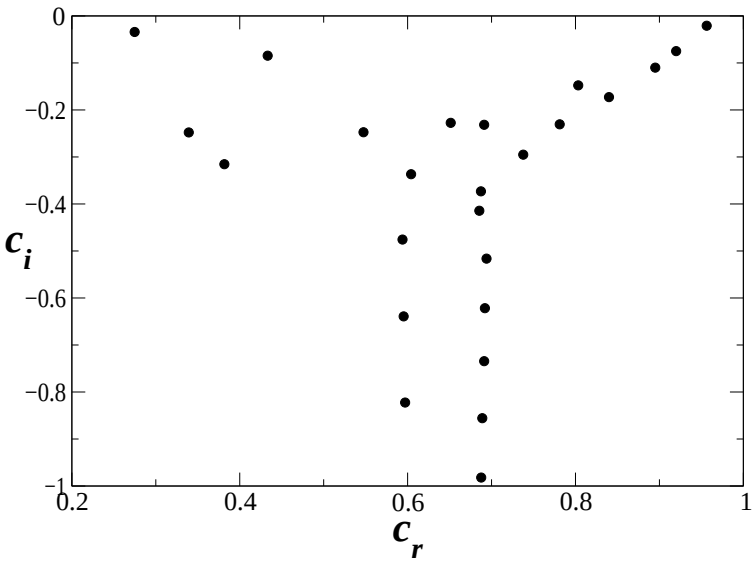

FIG. 3: Eigenvalue distribution generated for the Newtonian case of South and Hooper [23] with $m = 10$, $n = 1$, $\Gamma = 0$, G $= 0$, $Bn = 0$, $h^0 = 5/6$ and $\alpha = 2$.

D. Asymptotic analysis: $\alpha \to 0$, 'long-wave' limit

Here, we consider perturbations whose wavelength far exceeds the channel height. Our aim is to extend previous analyses to account for the effects of finite yield stress with $n = 1$ and to use these results as a further check on our numerical predictions; a similar analysis has previously been carried out for power-law fluids [19]. We use a regular perturbation expansion in powers of α for ψ_1, ψ_2, η and the eigenvalue, c:

$$(\psi_i, \eta, c) \sim (\psi_{i0}, \eta_0, c_0) + \alpha(\psi_{i1}, \eta_1, c_1) + O(\alpha^2), \quad i = 1, 2. \tag{21}$$

Substitution of Eq. (21) into Eqs. (11) and (12), and (13)-(18) yields a sequence of problems, which are solved order-by-order in powers of α.

The analysis is standard, and follows closely the procedure employed by Yiantsios and Higgins [6]. At leading order, the eigenfunctions are given by

$$\begin{aligned} \psi_{10} &= A_{00} + A_{01}y + A_{02}y^2 + A_{03}y^3, \\ \psi_{20} &= B_{00} + B_{01}y + B_{02}y^2 + y^3, \end{aligned} \tag{22}$$

and at $O(\alpha)$, the solutions read

$$\begin{aligned} \psi_{11} &= f_1(y) + A_{10} + A_{11}y + A_{12}y^2 + A_{13}y^3, \\ \psi_{21} &= f_2(y) + B_{10} + B_{11}y + B_{12}y^2 + y^3. \end{aligned} \tag{23}$$

The coefficients A_{ki} and B_{kj} $(i = 0, ..., 3)$, $(j = 0, ..., 2)$, $(k = 0, 1)$ are chosen such that Eqs. (13)-(18) are satisfied; we have set the coefficients of the terms proportional to y^3 in Eqs. (22) and (23) to unity without any loss of generality. The leading order and $O(\alpha)$ wave speeds, c_0 and c_1 are determined from Eq. (19).

We have found c_0 to be real and expressed by

$$c_0 = \frac{(dP/dx + 2Bn)\,(h^0 - 1)\,h^0\,[\beta_1\,(dP/dx) + 2\,(h^0 - 1)\,h^0 mBn]}{2\,[h^0\,(m - 1) - m]\,[\beta_2\,(dP/dx) - 6\,(h^0 - 1)\,h^0 mBn]} \tag{24}$$

where β_1 and β_2 are given by

$$\beta_1 \equiv \left[h^{0^2}(m - 1) - m\right]\left[h^0\left(h^0 - 2\right)(m - 1) + m\right], \tag{25}$$

$$\beta_2 \equiv h^{0^4} - 2h^0\left(h^0 - 1\right)\left[2 + \left(h^0 - 1\right)h^0\right]m + m^2\left(h^0 - 1\right)^4. \tag{26}$$

Hence c_0 depends on m, h^0, dP/dx as well as Bn, whereas the dependence on Re, r and G arises only at $O(\alpha)$. The expression obtained for c_1 as a function of system parameters is rather cumbersome and will not be reproduced here, but our $O(\alpha)$ analysis shows that c_1 is purely imaginary.

We conclude this section with a comparison of the results of the asymptotic analysis with the predictions of the numerical procedure. In Fig. 4, we show the numerical solution of the eigenvalue problem using the spectral collocation method and the predictions of the long-wave theory. Inspection of Fig. 4 reveals that excellent agreement is obtained in the limit of small α with deviations becoming apparent with increasing α, as expected. This inspires further confidence in the predictions of our numerical procedure.

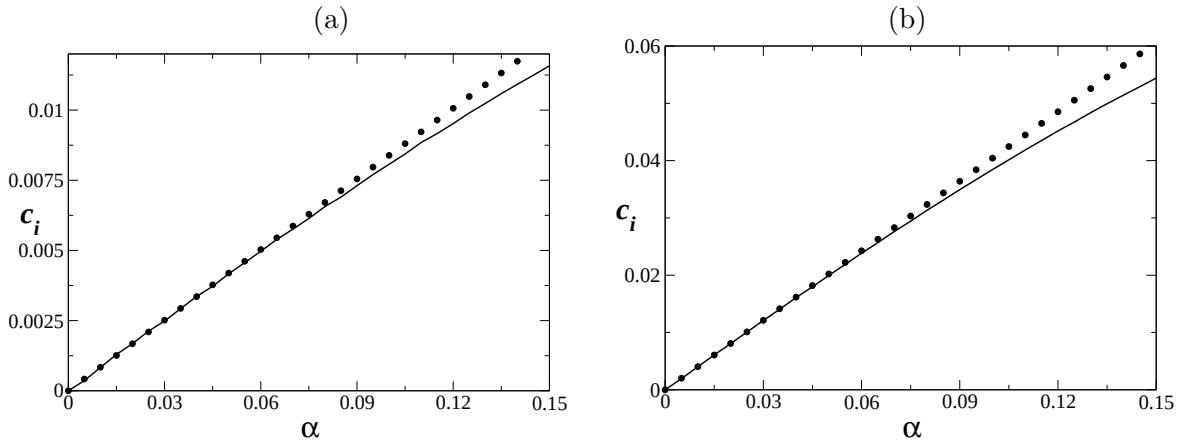

FIG. 4: Comparison of the numerical solution (solid lines) with the predictions of the long-wave analysis (dotted lines) in terms of the variation of the complex part of the phase speed, c_i, with the wavenumber, α. (a): $Bn = 0$, $m = 2$, $r = 1$, $G = 0$; (b): $Bn = 4$, $m = 5$, $r = 1.1$, $G = 10$. The rest of the parameters are Re $= 100$, $n = 1$ and $\Gamma = 0$.

III. RESULTS

In this section, we provide a discussion of our numerical results. Particular attention will be given to the effect of varying Bn and n on the linear stability characteristics since the influence of m, r, h^0, G and Γ on the stability of two-layer flows has been well studied.

A. Numerical results

1. *'Interfacial' mode*

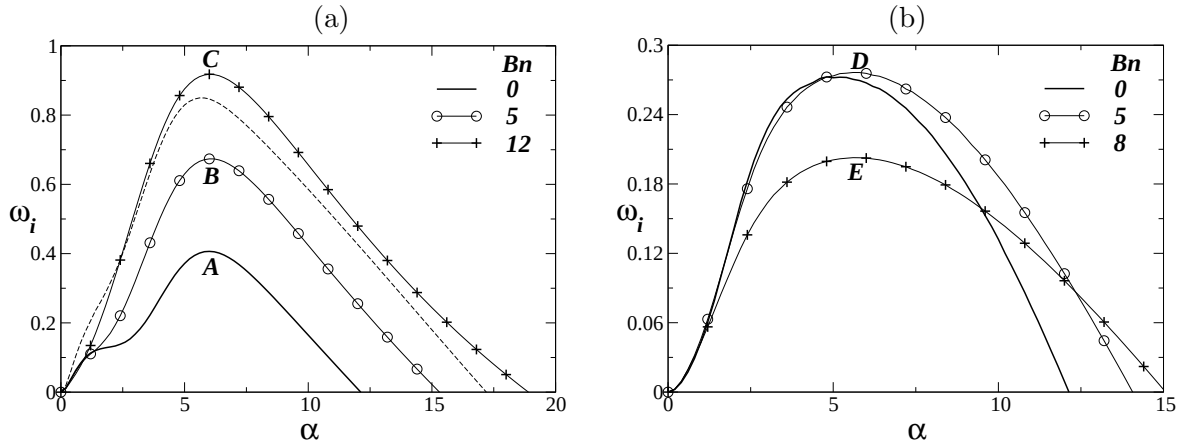

FIG. 5: The effect of varying the Bingham number, Bn, on the dispersion curves; (a): $h^0 = 0.5$ and (b): $h^0 = 0.2$. The rest of the parameters are $n = 1$, Re $= 100$, $m = 10$, $r = 1.1$ and $G = 10$ and $\Gamma = 1$. The labels 'A', 'B', 'C', 'D' and 'E' are used to designate maxima in the dispersion curves; the energy 'budgets' associated with these points are provided in table I. The dotted line in (a) shows the dispersion curve obtained by linearising about the base state for $Bn = 12$ and setting $Bn = 0$ in Eqs. (11) and (12).

We investigate first the effect of varying the Bingham number, Bn, on the linear stability characteristics. In Fig. 5, we plot numerically generated dispersion curves with $n = 1$, Re $= 100$, $m = 10$, $r = 1.1$ and $G = 10$ and $\Gamma = 1$. The choice of these parameters is reflective of physical situations wherein a Newtonian layer flows past a more dense and viscous layer of a Bingham fluid. The dispersion curves depicted in Fig. 5 are paraboloidal, and $\omega_i > 0$ over a finite band of wavenumbers, indicating the presence of a linear instability; there are also well-defined 'most-dangerous' and 'cut-off' modes that correspond to the values of α for which ω_i is maximal and beyond which $\omega_i > 0$, respectively. As shown in Fig. 5(a), increasing Bn for $h^0 = 0.5$ is destabilising, leading to an increase in the value of the wavenumber associated with the cut-off mode and an increase in the maximal growth rate; the most dangerous mode wavenumber appears to be weakly dependent on Bn. For $h^0 = 0.2$, however, increasing Bn increases the cut-off mode wavenumber but decreases the maximal growth rate; hence its overall effect is stabilising. The dotted line in Figure 5

shows the dispersion curve determined by performing a linear stability analysis of the base state associated with $Bn = 12$ but by setting $Bn = 0$ in Eqs. (11)-(12). The aim of this analysis is to isolate the effects of having a finite yield stress on the linear stability of the two-layer flow through its modification of the base state. Inspection of Fig. 5 reveals that such an analysis provides a reasonable approximation for low to intermediate wavenumbers but underestimates the maximal growth rate and the cut-off wavenumber.

TABLE I: Energy 'budgets' for the points labelled 'A', 'B', 'C', 'D' and 'E' in Fig. 5.

Point	REY_1	REY_2	DIS_1	DIS_2	TAN	TEN	HYD
A	-0.02	0.60	-1.40	-5.11	7.01	-0.13	0.04
B	-0.01	0.65	-0.84	-3.86	5.22	-0.21	0.06
C	0	0.78	-0.91	-4.37	5.77	-0.37	0.10
D	0	-0.13	-3.34	-16.34	22.88	-3.04	0.97
E	0	-0.90	-1.35	-14.90	19.38	-1.81	0.58

In order to identify the nature of unstable modes, we perform an energy decomposition following the methodology outlined in the Appendix [3]. The energy 'budgets' associated with the points labelled 'A', 'B' and 'C' in Fig. 5(a) at $\alpha = 6$ for $h^0 = 0.5$, $Bn = 0$, $Bn = 5$ and $Bn = 12$, respectively, are given in table I. Similarly, energy budgets for points 'D' and 'E' for $h^0 = 0.2$, which correspond to $\alpha = 5.6$, $Bn = 5$ and $Bn = 8$, respectively, are also provided in table I. The figures in table I represent the contribution arising from each term in Eq. (27) scaled by the total spatially-averaged rate of change of disturbance kinetic energy, KIN.

The energy decomposition reveals that, since TAN provides the largest positive contribution to KIN, the unstable modes examined are all of the 'interfacial' type, and, in this case, are driven by viscosity as well as density stratification. The Reynolds stress in the upper fluid, REY_2, is destabilising at $h^0 = 0.5$ and stabilising at $h^0 = 0.2$ and although the TAN and HYD contributions have increased substantially in the $h^0 = 0.2$ case, they are counter-balanced by large viscous dissipation, particularly in the upper fluid. It also appears that the increase in Bn from cases 'D' to 'E' is accompanied by a decrease in TAN and HYD and an increase in the stabilising contribution of REY_2; this may explain the overall stabilising effect of increasing Bn for $h^0 = 0.2$.

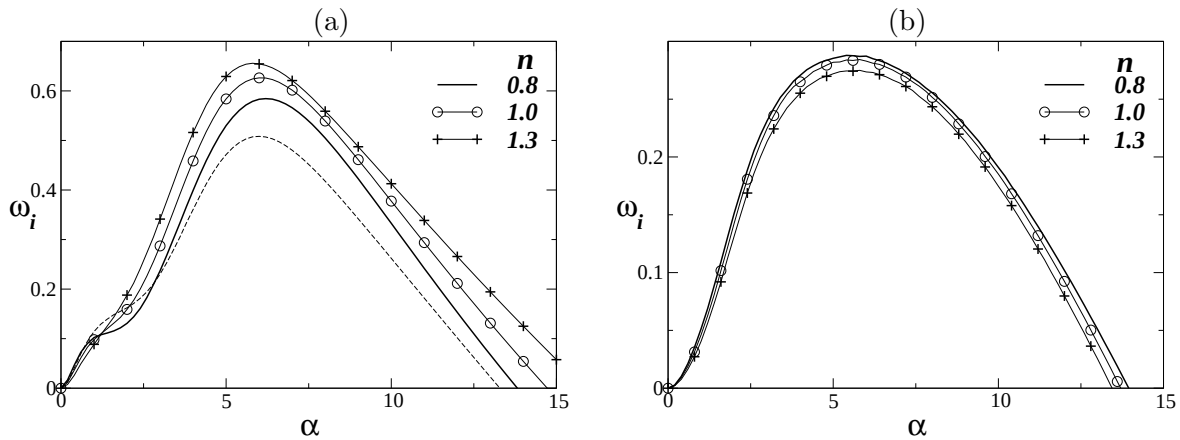

FIG. 6: The effect of varying the flow index, n, on the dispersion curves; (a): $h^0 = 0.5$ and (b): $h^0 = 0.2$. Here, $Bn = 4$ and the rest of the parameters are the same as in Fig. 5. The dotted line in (a) shows the dispersion curve obtained by linearising about the base state for $n = 0.8$ and setting $n = 1$ and $Bn = 0$ in Eqs. (11) and (12).

In Fig. 6, we investigate the effect of varying n on the stability characteristics for $Bn = 4$; the rest of the parameters remain unaltered from Fig. 5. For the larger h^0 values examined, decreasing the value of n, which reflects an increase in the shear-thinning tendency of the non-Newtonian layer has a stabilising effect. In contrast, for $h^0 = 0.2$, the opposite trend is seen, although the growth rates appear to be weakly dependent on variations in n in this case. We have also isolated the effect of power-law behaviour on the linear stability through its modification of the base state by linearising about a base state with $n = 0.8$ and setting $n = 1$ and $Bn = 0$ in Eqs. (11) and (12). A comparison of the results of this analysis, shown by the dotted line in Fig. 6, with the solid line, leads to similar conclusions to those drawn above: the simplified analysis underestimates the maximal growth and cut-off wavenumber.

The effect of varying the density ratio on the dispersion curves is examined in Fig. 7. As can be seen from Fig. 7(a), increasing the value of r appears to be destabilising in the range $0.1 < r < 2$. For the smallest values of r considered, the low-wavenumber cut-off is associated with a disturbance of intermediate wavenumber rather than $\alpha = 0$. As r is increased, the low-wavenumber cut-off and most dangerous modes shift towards $\alpha = 0$ and the dispersion curves become broader; the high-wavenumber cut-off appears to be relatively insensitive to variations in r in the range $0.1 < r < 2$, as shown in Fig. 7 (a). A further increase in r, however, leads to a decrease in the maximal growth rate but a shift of the

most dangerous and high-wavenumber cut-off modes towards larger wavenumbers, as shown in Fig. 7 (b). Although the results shown in Fig. 7 are for $h^0 = 0.5$, similar trends were observed for different h^0 values (not shown).

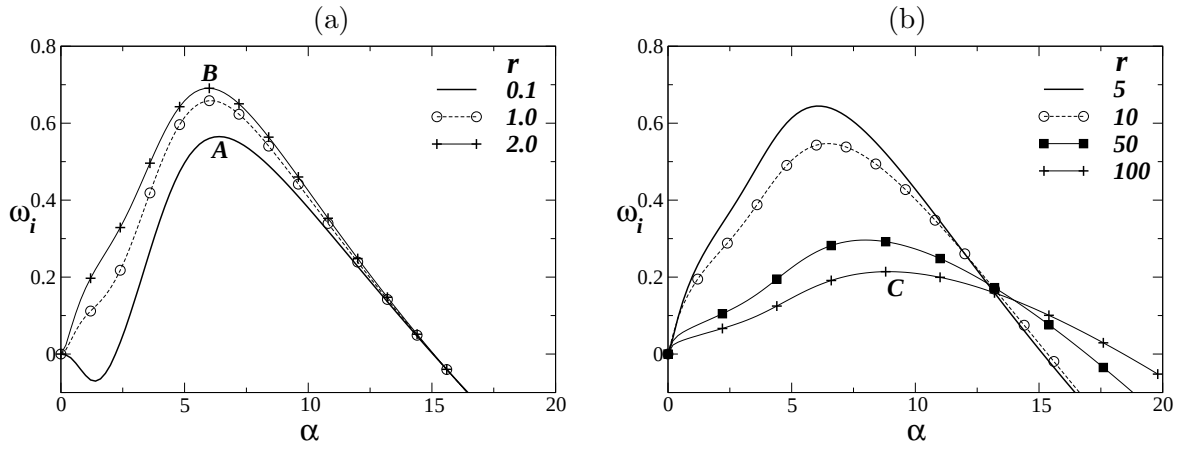

FIG. 7: Effect of varying the density ratio r on the dispersion curves for small, (a), and large, (b), r. The rest of the parameters are $Bn = 4$, $n = 1$, Re $= 100$, $m = 10$, $h^0 = 0.5$, $G = 0$ and $\Gamma = 1$. The labels 'A', 'B' and 'C' are used to designate global maxima in the dispersion curves associated with $r = 0.1, 2, 100$, respectively; the energy 'budgets' associated with these points are provided in table II.

The dependence of the stability characteristics on r can be explained by inspection of the energy 'budgets' of the points labelled 'A', 'B' and 'C' in Fig. 7, which are listed in table II. It is seen that the largest contribution to KIN is due to TAN, confirming the most unstable mode to be of 'interfacial' type. It can also be seen that REY_1 and REY_2 are negative for 'C' whereas REY_2 provides a positive contribution to KIN for points 'A' and 'B'. The corresponding values for the $Bn = 0$ case are given in brackets in table II. It is clearly seen that similar trends to those associated with the $Bn = 4$ case are also observed in the Newtonian case. It appears that the total viscous dissipation is largest at the extreme values of the density ratio examined and this may provide an explanation for the non-monotonic dependence on r shown in Fig. 7.

The effect of varying h^0, m and Γ in the presence of a finite yield stress is investigated next. As can be seen from Fig 8 (a), in which we show the dependence of the growth rate associated with the most dangerous mode, $(\omega_i)_{\max}$, on h^0, increasing the value of h^0, has a non-monotonic effect on $(\omega_i)_{\max}$: there exists an intermediate value for h^0 for which $(\omega_i)_{\max}$

TABLE II: Energy 'budgets' for the points labelled 'A', 'B', and 'C' in Fig. 7.

Point	REY_1	REY_2	DIS_1	DIS_2	TAN	TEN	HYD
A	0	0.68	-1.23	-5.35	7.14	-0.24	0
	(0)	(0.62)	(-1.78)	(-6.28)	(8.60)	(-0.16)	(0)
B	-0.02	0.65	-0.86	-3.78	5.19	-0.19	0
	(-0.03)	(0.65)	(-1.31)	(-4.69)	(6.52)	(-0.14)	(0)
C	-0.07	-0.36	-0.49	-7.12	9.04	-0.01	0
	(-0.12)	(-0.30)	(-0.80)	(-7.51)	(9.73)	(-0.01)	(0)

is maximised. The dependence of $(\omega_i)_{\max}$ on m is similarly non-monotonic, as demonstrated in Fig. 8 (b). The presence of a yield stress amplifies the non-monotonic trends already present in the Newtonian case, which are also shown in Fig. 8, particularly for variations in h^0. We have also found that increasing the relative significance of the interfacial tension effects to be stabilising monotonically (not shown): an increase in Γ decreases the value of the wavenumber associated with the cut-off mode, as expected.

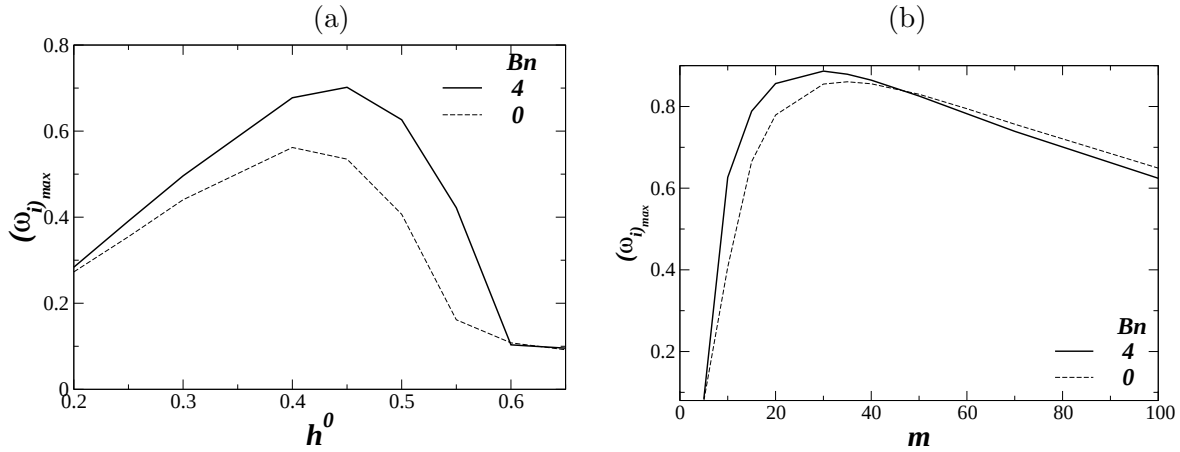

FIG. 8: Effect of varying the thickness ratio h^0, (a), and viscosity ratio m, (b), on the growth rate associated with the most dangerous mode, $(\omega_i)_{\max}$ in the presence and absence of a yield stress. The rest of the parameters are $n = 1$, $h^0 = 0.5$, Re $= 100$, $m = 10$, $r = 1.1$, $G = 10$ and $\Gamma = 1$.

We have also explored the effect of increasing Re on the stability characteristics in the presence of non-Newtonian rheology. We show in Fig. 9 the parametric dependence of the dispersion curves on Re for $Bn = 0$ and $Bn = 12$. Panel (a), which depicts the curves associated with the 'interfacial' mode, demonstrates the destabilising influence of

inertia: increasing Re leads to an increase in the maximal growth rate, and increasing Bn reinforces this trend and further destabilises the flow. **We have carried out an energy decomposition for the** $\mathrm{Re} = 100$ **and** $\mathrm{Re} = 1000$ **cases, the results of which are shown in table III. Inspection of these results reveals that the increase in TAN for** $Bn = 0$ **is counterbalanced by a substantial increase in viscous dissipation; furthermore, in the case of** $\mathrm{Re} = 1000$ **and** $Bn = 0$ **there appears to be a substantial increase in TEN, which is stabilising. These effects conspire to widen the interval of "unstable" wavenumbers for** $Bn > 0$**.**

In panel (b), we show dispersion curves generated by plotting the imaginary part of the second leading eigenvalue against α for the same parameters as in (a). These curves are therefore associated with another mode, distinct from the 'interfacial' mode. This mode, which will be shown below to be of the 'shear' type, has a band of α for which $\omega_i > 0$ at $\mathrm{Re} = 20000$. Hence, at sufficiently large Re, there are two unstable modes. In the following section, we shall focus attention on the least stable of the two: the 'shear' mode.

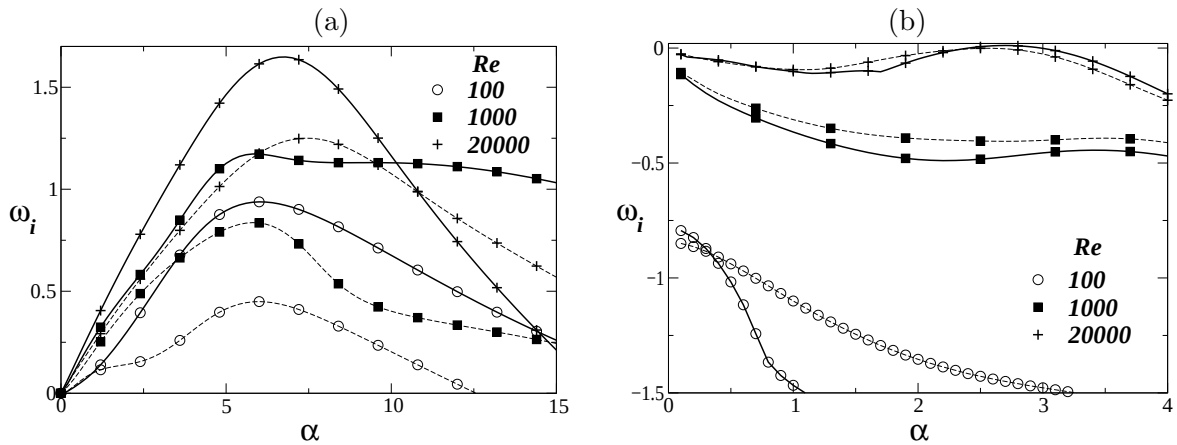

FIG. 9: Effect of varying the Reynolds number, Re, on the dispersion curves generated by plotting the imaginary parts of the two leading eigenvalues against α with $Bn = 0$ (dashed lines) and $Bn = 12$ (solid lines). The rest of the parameters are $n = 1$, $m = 10$, $r = 1$, $h^0 = 0.5$, $G = 0$ and $\Gamma = 1$.

2. *Shear mode*

Here, we consider $\mathrm{Re} \in [10^4 : 5 \times 10^4]$ and find another unstable mode in addition to the 'interfacial' mode. The neutral stability curves of the second unstable mode for different

TABLE III: **Energy 'budgets' for** $\mathrm{Re} = 100, 1000$**,** $\alpha = 15$ **and the parameter values used to generate Fig. 9.**

Re	Bn	REY_1	REY_2	DIS_1	DIS_2	TAN	TEN	HYD
100	12	0	-0.38	-0.50	-10.03	11.92	-0.02	0
	0	0.01	-1.13	-3.28	-19.67	25.06	0.02	0
1000	12	-0.01	0.34	-0.90	-1.28	1.93	-1.09	0
	0	-0.04	11.13	-39.87	-70.32	112.09	-13.98	0

Bingham numbers are shown in Fig. 10(a) and (b). It is seen that the presence of a finite yield stress is destablising for $h^0 = 0.5$ and stablising for $h^0 = 0.2$. We see that in the former case this coincides with the unstable waves being shorter than in the Newtonian case. These trends are also evident upon inspection of the dispersion curves shown in Fig. 12, which furthermore demonstrate that increasing Bn has a destabilising influence on the 'interfacial' mode for $h^0 = 0.2$ and $h^0 = 0.5$. Here, it is also seen that the second mode is considerably less unstable than the 'interfacial' modes even at large Re and mode competition [24] is not an issue here. In spite of this large disparity in growth rate, these unstable modes can still be observed experimentally since their dimensional growth rate is not excessively small; their effect on the stability of the flow cannot therefore be neglected [25].

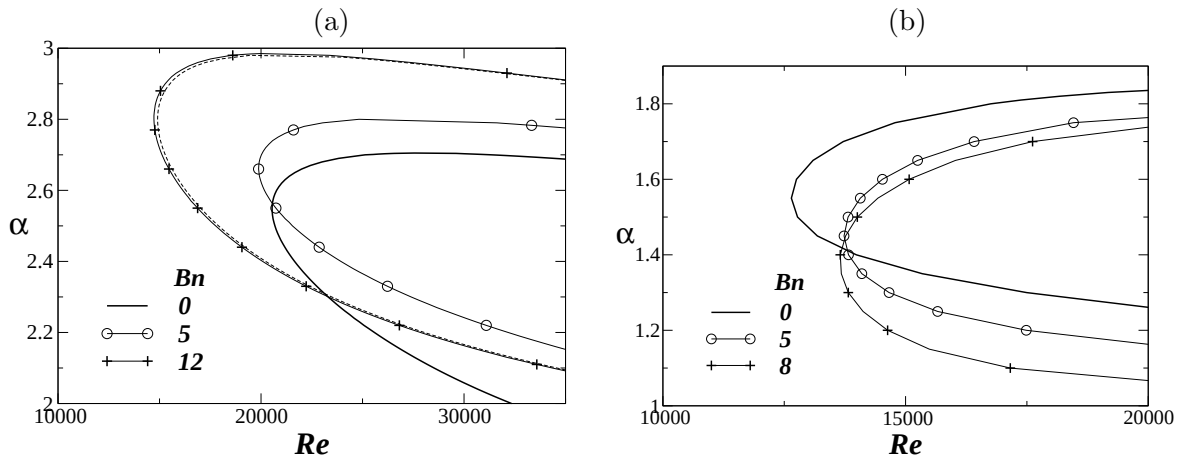

FIG. 10: The effect of varying Bn on the neutral stability curves of the 'shear' mode; (a): $h^0 = 0.5$ and (b) $h^0 = 0.2$. The rest of the parameters are $n = 1$, $m = 10$, $r = 1$, $G = 0$, and $\Gamma = 1$.

In order to investigate this behaviour in more detail, we compute the energy budgets of the most dangerous modes, labelled 'A'-'D' in Fig. 12; these are listed in table IV. Inspection

of table IV reveals that, for both $h^0 = 0.5$ and $h^0 = 0.2$, the largest positive contribution to the spatially-averaged rate of change of disturbance kinetic energy is due to the Reynolds stresses in the upper fluid. This indicates that the second unstable mode corresponds to a 'shear' mode. **In Fig. 11, we also show the cross-stream structure of ψ, which contrasts the shape of the stream function associated with an 'interfacial' mode and the second unstable, 'shear' mode.**

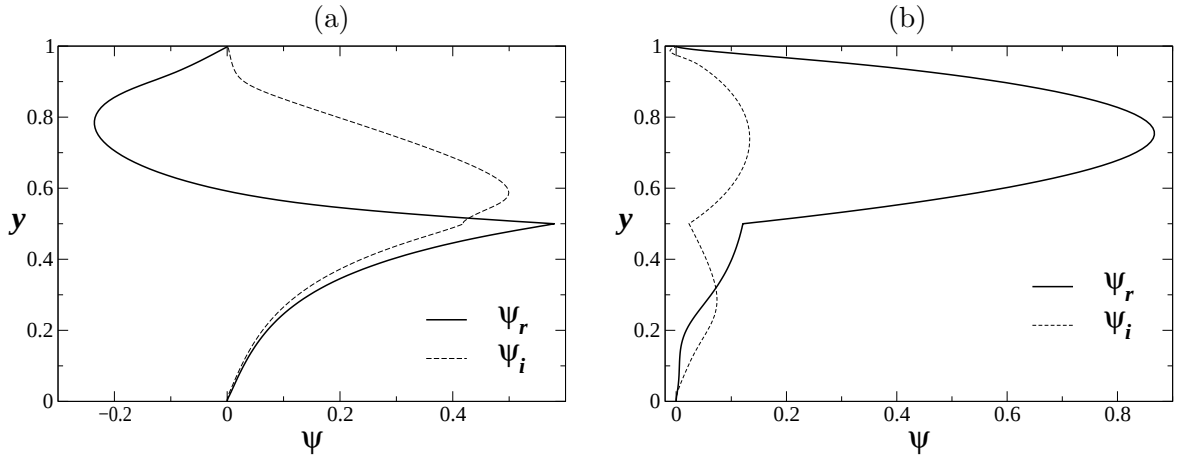

FIG. 11: **The cross-stream structure of the real and imaginary parts of ψ for which parameters? shown in (a) and (b), which depicts examples of the stream function associated with an 'interfacial' and a 'shear' mode, respectively.**

We have verified that for cases wherein the viscosity of the lower fluid is less than that of the upper fluid, the shear mode is associated with the lower fluid (evidence of three unstable shear modes was only found in preliminary results at Reynolds number values that are beyond the scope of this study). It is also evident from Fig. 12 and table IV that an increase in Bn for $h^0 = 0.5$ is destabilising despite a concomitant decrease in REY_2; this is due to a decrease in total viscous dissipation and in the stabilising contribution of REY_1. For $h^0 = 0.2$, the stability characteristics appear to be weakly-dependent on variations in Bn.

In Figs. 13 and 14, we show the effect of varying the flow index n on the neutral stability and dispersion curves of the 'shear' mode. It is seen that increasing n is destabilising for both $h^0 = 0.2$ and $h^0 = 0.5$; this effect becomes more pronounced with increasing h^0. This can also be understood by examining the energy budgets of the modes labelled 'A'-'D' in Fig. 14 that are listed in table V: increasing n for $h^0 = 0.5$ leads to a decrease in the total

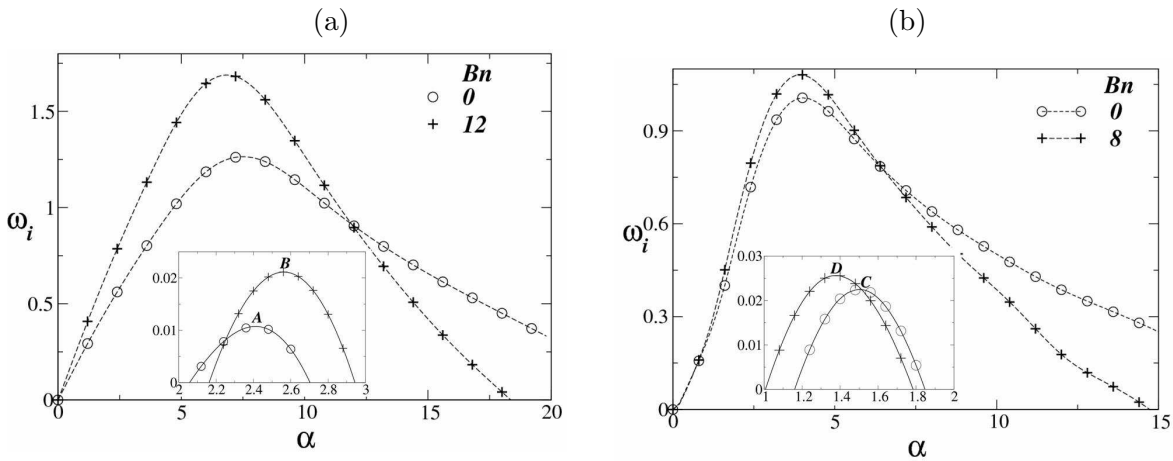

FIG. 12: **Effect of varying Bn on the dispersion curves with** Re = 30000**; (a)** $h^0 = 0.5$ **and (b)** $h^0 = 0.2$**. The rest of the parameters are the same as in Fig 10. The curves associated with the 'shear' modes are shown in the insets of panels (a) and (b).**

TABLE IV: Energy budgets for the points labelled 'A'-'D' in Fig. 12.

Point	REY_1	REY_2	DIS_1	DIS_2	TAN	TEN	HYD
A	-2.37	9.21	-0.32	-4.56	0.05	-1.00	0
B	-0.14	2.54	-0.03	-1.34	0.04	-0.06	0
C	0.01	1.50	-0.03	-0.47	0.02	-0.04	0
D	0.01	1.81	-0.27	-0.46	0.05	-0.13	0

viscous dissipation and the stabilising contribution from REY_1, which counterbalance the large decrease in REY_2; this leads to an overall destabilising effect. We also show in Fig. 13(a) that linearising about a base state associated with $n = 0.8$ and $Bn = 4$ and setting $n = 1$ and $Bn = 0$ in Eqs. (11) and (12) underestimates the critical Re.

We have also investigated the effect of m and r on the neutral stability curves of the 'shear' mode in the presence of a yield stress. As shown in Figs. 15 and 16, increasing m and decreasing r is destabilising, leading to lower threshold Re values. These trends are insensitive to changes in h^0. The non-monotonic dependence on r associated with the 'interfacial' mode (see Fig. 7) is absent in the case of the 'shear' mode.

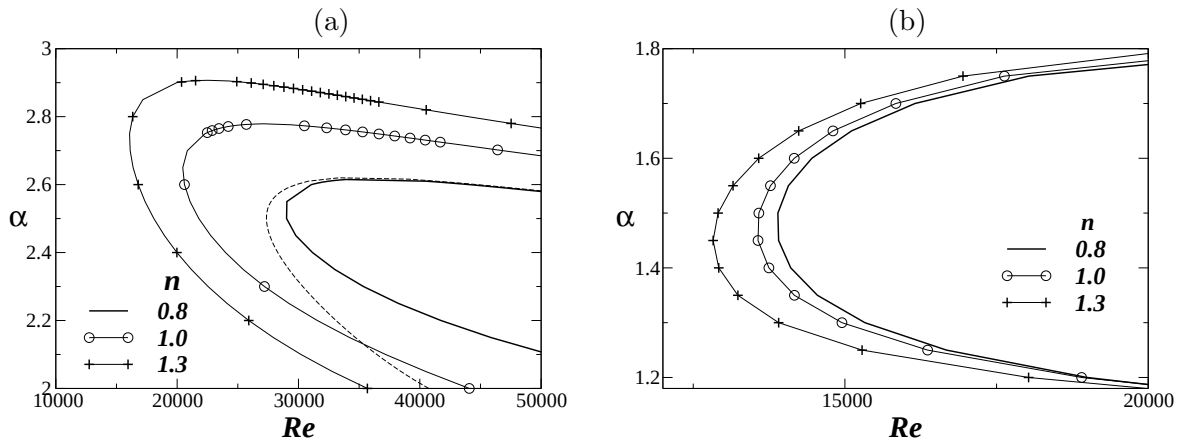

FIG. 13: The effect of varying the flow index, n, on the neutral stability curve of the 'shear' mode; (a) $h^0 = 0.5$ and (b) $h^0 = 0.2$. The rest of the parameters are $r = 1$, $Bn = 4$, $m = 10$, $G = 0$, and $\Gamma = 1$. The dotted line in (a) was obtained by linearising about a base state with $n = 0.8$ and $Bn = 4$ and by setting $n = 1$ and $Bn = 0$ in Eqs. (11) and (12).

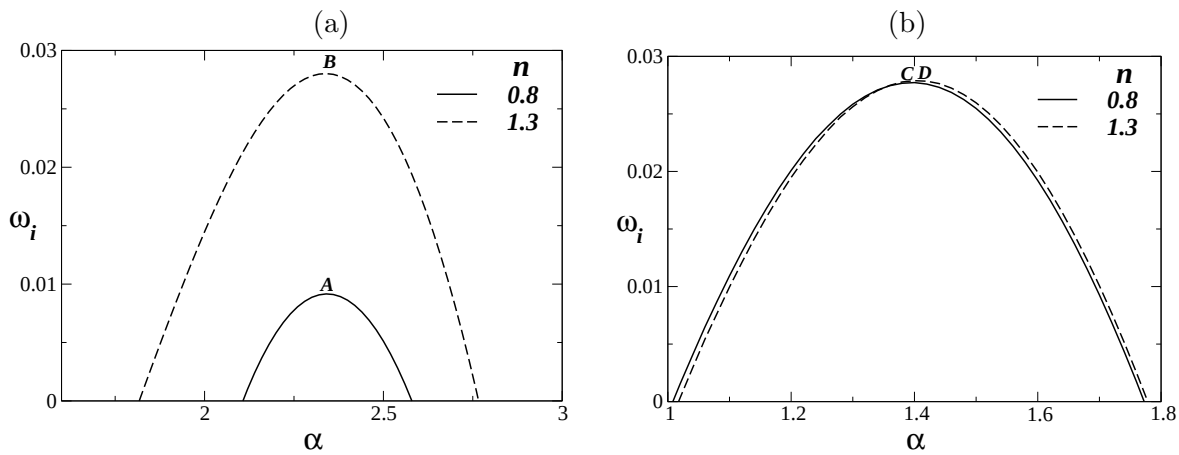

FIG. 14: The effect of varying n on the dispersion curves with Re = 50000; (a) $h^0 = 0.5$ and (b) $h^0 = 0.2$. The rest of the parameters are same as Fig 13.

IV. CONCLUSIONS

We have investigated the linear stability of two-layer pressure-driven flow in a channel. We have considered the case in which the upper layer is Newtonian while the lower one is non-Newtonian, whose rheological behaviour is described by a Herschel-Bulkley model. This model incorporates the effects of finite yield stress as well as power-law behaviour. In order to examine the stability characteristics of the flow, we have derived an Orr-Sommerfeld

TABLE V: Energy budgets for the points labelled 'A'-'D' in Fig. 14.

Point	REY_1	REY_2	DIS_1	DIS_2	TAN	TEN	HYD
A	-4.25	10.89	-0.41	-4.30	0.05	-0.98	0
B	-0.24	2.39	-0.02	-0.84	0.01	-0.29	0
C	0.01	1.36	-0.04	-0.29	0.02	-0.06	0
D	0.01	1.33	-0.02	-0.28	0.01	-0.05	0

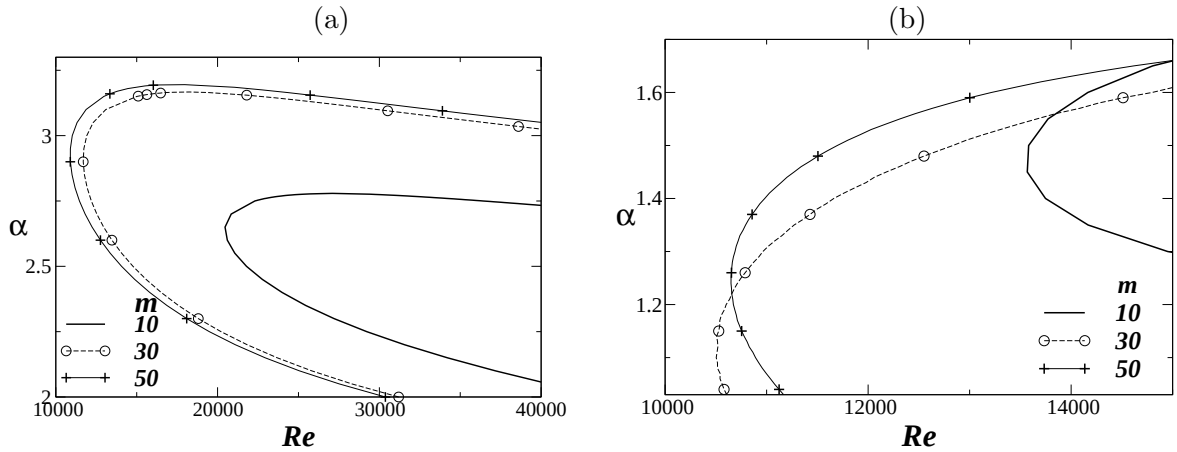

FIG. 15: The effect of varying m on the neutral stability curves of the 'shear' mode; (a) $h = 0.5$ and (b) $h = 0.2$. The rest of the parameters are $n = 1$, $Bn = 4$, $r = 1$, $G = 0$, and $\Gamma = 1$.

eigenvalue problem, which features a pair of coupled fourth-order, ordinary differential eigenvalue equations for the stream functions in both layers; here, the eigenvalue corresponds to the wave speed. These equations are parameterised by a Bingham number, Bn, and a flow index, n, which characterise the relative significance of the yield stress and power-law properties of the non-Newtonian fluid, respectively, in addition to viscosity, density and thickness ratios, and gravitational and interfacial tension parameters. The Orr-Sommerfeld problem was solved using a perturbation technique valid for low wavenumbers and numerically using a spectral collocation for arbitrary wavenumbers; only two-dimensional perturbations were considered. Comparisons of our numerical predictions with those of our asymptotic analysis and with published results yielded excellent agreement.

Our results indicate that increasing the values of Bn and n, which reflect the relative significance of yield stress and power-law behaviour, respectively, promote instability. The effect of these parameters become particularly pronounced

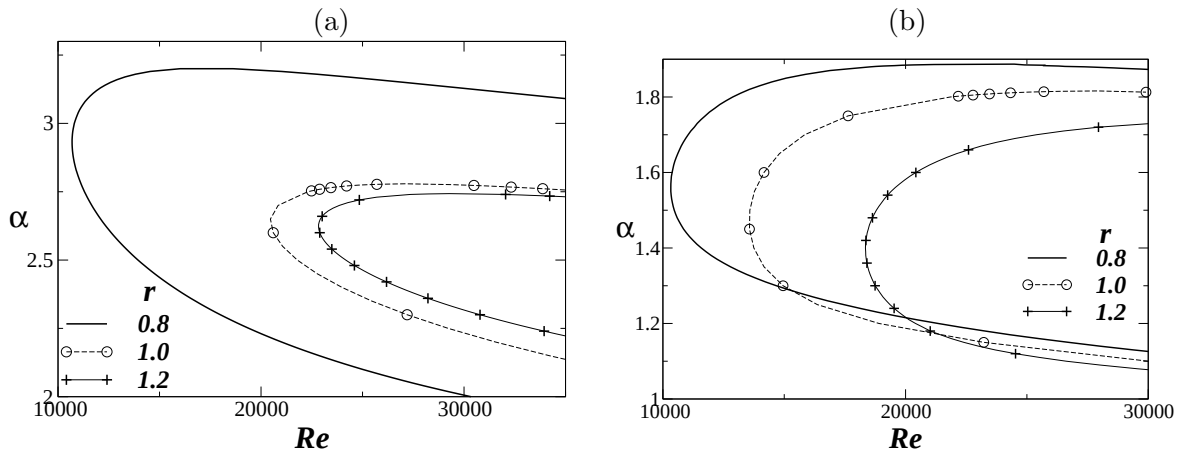

FIG. 16: The effect of varying r on the neutral stability curves of the 'shear' mode; (a) $h = 0.5$ and (b) $h = 0.2$. The rest of the parameters are $n = 1$, $Bn = 4$, $m = 10$, $G = 0$, and $\Gamma = 1$.

at relatively large values of the non-Newtonian layer thickness. At small and moderate values of the Reynolds number, a single unstable mode is found; a second mode becomes unstable at large values of Re. An energy balance shows that the former is an 'interfacial' mode, whereas the latter corresponds to a 'shear' mode associated with the least viscous fluid. In all cases studied, the growth rate of the 'interfacial' mode was found to greatly exceed that of the 'shear' mode. This indicates that the former would be the most likely to be observed experimentally although one cannot rule out the possibility that the latter may also be observed since its growth is not vanishingly small. It is important to note that the results could only partly be explained by an analysis based on Newtonian fluids wherein the change in the base-state velocity profile is accounted for. Hence the full non-Newtonian analysis is required for an accurate solution of the stability problem.

Acknowledgements

The authors would like to acknowledge the support of the DTI, through grant number TP//ZEE/6/1/21191. Useful discussions with Prof. C. J. Lawrence are also acknowledged.

Appendix: Energy balance

We provide here a concise derivation of the energy equation, extending the balance derived by Boomkamp and Miesen [3] (see also references therein), amongst others, to the non-Newtonian system studied in the present paper. Decomposition of this equation into energy production and dissipation terms allows one to isolate the mechanisms by which energy is transferred from the base flow to the disturbances. This decomposition also allows one to determine the type of instability mode, whether 'interfacial' or 'shear'.

The energy equation is derived by taking the inner product of the horizontal and vertical components of the Navier-Stokes equations with their respective velocity components. The resultant equation is then averaged over the wavelength, λ, and integrated over the height of channel. Application of this procedure to the equations in both fluids, addition of the resultant equations and making use of the Gauss-divergence theorem yields

$$\sum_{j=1}^{2} KIN_j = \sum_{j=1}^{2} DIS_j + \sum_{j=1}^{2} REY_j + INT, \tag{27}$$

where subscript $j = 1$ and $j = 2$ represent the lower (non-Newtonian) and upper (Newtonian) fluids, respectively. In Eq. (27), KIN_j, DIS_j and REY_j are expressed by

$$KIN_j = \frac{r_j}{\lambda}\frac{\mathrm{d}}{\mathrm{d}t}\int_{a_j}^{b_j} \mathrm{d}y \int_0^{\lambda} \mathrm{d}x \left[\frac{1}{2}\left(\hat{u}_j^2 + \hat{v}_j^2\right)\right], \tag{28}$$

$$DIS_j = -\frac{1}{\lambda \mathrm{Re}}\int_{a_j}^{b_j} dy \int_0^{\lambda} \mu_j \mathrm{d}x \left[2\left(\frac{\partial \hat{u}_j}{\partial x}\right)^2 + \left(\frac{\partial \hat{u}_j}{\partial y} + \frac{\partial \hat{v}_j}{\partial x}\right)^2 + 2\left(\frac{\partial \hat{v}_j}{\partial y}\right)^2\right], \tag{29}$$

$$REY_j = \frac{r_j}{\lambda}\int_{a_j}^{b_j} \mathrm{d}y \int_0^{\lambda} \mathrm{d}x \left[-\hat{u}_j \hat{v}_j \frac{\partial U_j}{\partial y}\right]; \tag{30}$$

for the lower fluid, $\mu_1 = m\Pi^{n-1} + Bn\Pi^{-1}$, $r_1 = r$, $a_1 = 0$, $b_1 = h$ and for the upper fluid, $\mu_2 = 1$, $r_2 = 1$, $a_2 = h$, $b_2 = 1$. KIN_j represents the spatially averaged rate of change of disturbance kinetic energy and is proportional to the growth rate. DIS_j represents the viscous dissipation of energy and is always negative; note the presence of μ_1 inside the integrand for the non-Newtonian fluid. $INT = NOR + TAN$ is associated with the existence of an interface and is decomposed into NOR and TAN, the work done by the velocity and stress disturbances in the directions normal and tangential to the interface, respectively. NOR is given by

$$NOR = \frac{1}{\lambda \mathrm{Re}}\int_0^{\lambda} [\hat{v}_1 \tau_1^{yy} - \hat{v}_2 \tau_2^{yy}]_h \mathrm{d}x, \tag{31}$$

which is further decomposed into TEN and HYD, work done against the deformation of the interface due to interfacial tension and gravity respectively:

$$NOR \equiv TEN + HYD = \frac{1}{\lambda \mathrm{Re}} \int_0^\lambda \left[\hat{v}\Gamma\hat{\eta}_{xx}\right]_{y=h} \mathrm{d}x + \frac{1}{\lambda \mathrm{Re}} \int_0^\lambda \left[\hat{v}G\hat{\eta}\right]_{y=h} \mathrm{d}x. \tag{32}$$

TAN, is given by

$$TAN = \frac{1}{\lambda \mathrm{Re}} \int_0^\lambda \left[u_1\tau_1^{xy} - u_2\tau_2^{xy}\right]_h \mathrm{d}x. \tag{33}$$

In Eqs. (31) and (33), the components of stress tensor are defined as

$$\tau_j^{xy} = \mu_j \left(\frac{\partial u_j}{\partial y} + \frac{\partial v_j}{\partial x}\right), \quad \text{and} \quad \tau_j^{yy} = -p_j + 2\mu_j \frac{\partial v_j}{\partial y}, \tag{34}$$

where p_j denote the pressure disturbances.

---

[1] R. B. Bird, G. C. Dai, and B. J. Yarusso, "The rheology and flow of viscoplastic materials," Revs Chem. Eng. **1**, 1 (1982).

[2] P. H. T. Uhlherr *et al.*, "The shear-induced solid-liquid transition in yield stress materials with chemically diffefrent structures," J. Non-Newt. Fluid Mech. **125**, 101 (2005).

[3] P. A. M. Boomkamp and R. H. M. Miesen, "Classification of instabilities in parallel two-phase flow," Int. J. Multiphase Flow **22**, 67 (1996).

[4] C.-S. Yih, "Instability due to viscosity stratification," J. Fluid Mech. **27**, 337 (1967).

[5] S. G. Yiantsios and B. G. Higgins, "Numerial solution of eigenvalue problems using the compound matrix-method," J. Comp. Phys. **74**, 25 (1988).

[6] S. G. Yiantsios and B. G. Higgins, "Linear stability of plane Poiseuille flow of two superposed fluids," Phys. Fluids **31**, 3225 (1988).

[7] A. P. Hooper and W. G. C. Boyd, "Shear-flow instability at the interface between two viscous fluids," J. Fluid Mech. **128**, 507 (1983).

[8] T. W. Kao and C. Park, "Experimental investigations of stability of channel flows. Part II. Tw-layered co-current flow in a rectangular channel," J. Fluid Mech. **52**, 401 (1972).

[9] A. P. Hooper and R. Grimshaw, "Nonlinear instability at the interface between two viscous fluids," Phys. Fluids **28**, 37 (1985).

[10] J. C. Miller and J. M. Rallison, "Interfacial instability between sheared elastic liquids in a channel," J. Non-Newt. Fluid Mech. **143**, 71 (2007).

[11] J. C. Miller and J. M. Rallison, "Instability of coextruded elastic liquids at high Weissenberg number," J. Non-Newt. Fluid Mech. **143**, 88 (2007).

[12] R. Valette, P. Laure, Y. Demay, and J. F. Agassant, "Convective linear stability analysis of two-layer coextrusion flow for molten polymers," J. Non-Newt. Fluid Mech. **121**, 41 (2004).

[13] R. Valette, P. Laure, Y. Demay, and J. F. Agassant, "A theoretical and experimental investigation of convective instabilities in a two-layer coextrusion flow of molten polymers," Proc. XIVth Congr. on Rheology F105 1 (2004).

[14] P. Laure *et al.*, "Linear stability of multilayer plane Poiseuille flows of Oldroyd B fluids," J. Non-Newt. Fluid Mech. **71**, 1 (1997).

[15] W. J. Sang, "Interfacial instabilities in plane Poiseuille flow of two stratified viscoelastic fluids with heat transfer. Part 1. Evolution equation and stability analysis," J. Fluid Mech. **299**, 241 (1995).

[16] I. A. Frigaard, "Super-stable parallel flows of multiple visco-plastic fluids," J. Non-Newt. Fluid Mech. **100**, 49 (2001).

[17] I. A. Frigaard, S. D. Howison, and I. J. Sobey, "On the stability of Poiseuille flow of a Bingham fluid," J. Fluid Mech. **263**, 133 (1994).

[18] A. Pinarbasi and A. Liakopoulos, "Stability of two-layer Poiseulle flow of Carreau-Yasuda and Bingham-like fluids," J. Non-Newt. Fluid Mech. **57**, 227 (1995).

[19] B. Khomami, "Interfacial stability and deformation of two stratified power-law fluids in plane Poisuille flow. Part I. Stability Analysis," J. Non-Newt. Fluid Mech. **36**, 289 (1990).

[20] B. Khomami, "Interfacial stability and deformation of two stratified power-law fluids in plane Poisuille flow. Part II. Interface deformation," J. Non-Newt. Fluid Mech. **37**, 19 (1990).

[21] C. Canuto, M. Y. Hussaini, A. Quarteroni, and T. A. Zhang, *Spectral Methods in Fluid Dynamics*, 1st ed. (Springer-Verlag, ADDRESS, 1987), pp. 65–70.

[22] K. C. Sahu and R. Govindarajan, "Stability of flow through a slowly diverging pipe," J. Fluid Mech. **531**, 325 (2005).

[23] M. J. South and A. P. Hooper, "Linear growth in two-fluid plane Poiseuille flow," J. Fluid Mech. **381**, 121 (1999).

[24] P. Yecko, S. Zaleski, and J.-M. Fullana, "Viscous modes in two-phase mixing layers," Phys. Fluids **14**, 4115 (2002).

[25] P. A. M. Boomkamp, R. H. M. Miesen, and G. V. Beijnon, J. Comp. Phys. **132**, 191 (1997).